Post-print version https://doi.org/10.1088/1361-6528/ac3861

Electrical impedance sensing of organic pollutants with ultrathin graphitic membranes

Marian Baah[1*], Afifa Rahman[1*], Sarah Sibilia[2], Gianmarco Trezza[2], Luigi Ferrigno[2], Laura Micheli[3], Antonio Maffucci[2], Ekaterina Soboleva[4], Yuri Svirko[1], Polina Kuzhir [1,5]

[1] Department of Physics and Mathematics, Institute of Photonics, University of Eastern Finland, Joensuu, Finland
[2] Department of Electrical and Information Engineering, University of Cassino and Southern Lazio, Cassino, Italy
[3] Department of Chemical Science and Technologies, University of Rome "Tor Vergata", Rome, Italy
[4] Lappeenranta-Lahti University of Technology LUT, Lappeenranta, Finland
[5] Institute for Nuclear Problems of Belarusian State University, 220006 Minsk, Belarus

E-mail: marian.baah@uef.fi, polina.kuzhir@uef.fi

Received xxxxxx
Accepted for publication xxxxxx
Published xxxxxx

Abstract

In this paper we propose an original approach for the real-time detection of industrial organic pollutants in water. It is based on the monitoring of the time evolution of the electrical impedance of low-cost graphitic nanomembranes. The developed approach exploits the high sensitivity of the impedance of 2D graphene-related materials to the adsorbents. We examined sensitivity of the nanomembranes based on Pyrolyzed Photoresist (PPF), Pyrolytic Carbon (PyC), and Multilayer Graphene (MLG) films. In order to realize a prototype of a sensor capable of monitoring the pollutants in water, the membranes were integrated into an ad-hoc printed circuit board. We demonstrated the correlation between the sensitivity of the electric impedance to adsorbents and the structure of the nanomembranes, and revealed that the amorphous PyC, being most homogeneous and adhesive to the SiO_2 substrate, is the most promising in terms of integration into industrial pollutants sensors.

Keywords: graphitic films, electrical impedance spectroscopy, environmental sensors.

* M.B. and A.R. contributed equally to this paper.

1. Introduction

The implementation of a qualitative and quantitative detection of toxic and/or hazardous organic substances in water is a key-challenge to face in order to address the United Nations Sustainable Development goals. The development of low-cost and compact sensing systems capable of detection in-situ and in real time the presence of organic pollutants in water would be a significant breakthrough in the water monitoring technology. The recently demonstrated opportunity to improve the conventional chemical sensing techniques by combining them with advanced electrochemical or biological detection methods [1] demands moving the analysis of the water quality from the lab to the situ and achieving the real-time monitoring [2]. Recently, electrochemical methods, such as Voltammetry (VA), have provided impressive sensing performance due to the outstanding response provided by 2D nanomaterials, based on carbon or on other elements [3]-[7]. These methods can be, in principle, proposed to implement low-cost and in-situ monitoring systems. However, VA-based methods are not suitable for a time-continuous monitoring, due to the well-known problem of the passivation of the electrodes in presence of organic pollutants, such as the quinones. Indeed, when the quinones are present, during the electrochemical measurements it is possible to detect the generation of a coating on the working electrode and the subsequent formation of a polymer, whose nature depends on

the presence or absence of oxygen. These coatings prevent the regular redox process of quinones from taking place on the surface of the electrode, and are generated regardless of the used electrode material, or the presence of O_2 in solution [8]-[9]. Indeed, this phenomenon allows using the electrode only one time, since after a first measurement its surface is modified due to the quinone electrochemical polymerization [10].

In this paper, we propose an alternative approach that has the potential to overcome the above limitations and to provide a real-time *in situ* monitoring solution. With this goal, we have chosen benzoquinone to assess the response of the proposed approach with respect to the challenging class of industrial organic pollutants of quinones.

The proposed method is based on the possibility of detecting the presence of organic pollutants by measuring the variation induced on the electrical impedance of suitable sensing elements. This approach, belonging to the class of the Electrical Impedance Spectroscopy (EIS) techniques [11], has been recently applied to the monitoring of the state of health of filters for water remediation [12]-[14].

To realize a sensor based on the above approach, one of the major challenges is to find a simple, reliable and feasible sensing material, which will be suitable for integration into a portable device and will be able to meet the sensitivity and selectivity requirements. The outstanding electrochemical performance of graphene and other thin carbon films [4] offers new horizons for the environmental sensing [14]-[15]. This is mainly because 2D nanomaterials and their derivatives possess the highest surface to volume ratio, when almost each atom can be considered as a surface one, and this dramatically increases the ability to adsorb external molecules. The extremely high sensitivity of their electrical and electrochemical properties to the adsorption of external substances results in exceptionally high sensing performance of such materials. For this reason, they have been recently used to realize the sensing elements in electrochemical characterizations, such as Cyclic Voltammetry (CV) [16], as well as in electrical characterization, such as EIS [11].

The implementation of the recently demonstrated outstanding properties of exfoliated graphene sheets in industrial applications is unrealistic given the high production costs and the limited yields. Correspondingly, nowadays attention is paid on low-cost graphene-related nanomaterials, including graphene nanoplatelets, graphene oxide, pyrolytic carbon and carbon nanotubes [4], [12], [17]-[18]. These materials have been successfully used in environmental applications, such as sorbents [19], filters for air and water remediation [20]-[21], high-flux membranes [22], and for renewable energy applications [23].

In this paper, we report the implementation of thin graphitic membranes, i.e. Pyrolyzed Photoresist [24], Pyrolytic Carbon [25], and Multilayer Graphene in EIS based sensors. Depending on the synthesis method, graphitic films may differ by conductivity and crystallinity (from highly ordered multi-layered graphene to almost amorphous pyrolyzed resist and pyrolytic carbon) being composed of either large (up to several microns) or small (5-10 nm) graphene flakes.

The prototype of the EIS-based sensing system was created by integrating a graphitic nanomembrane into a printed circuit board (PCB), which is an interface between the sensing elements and the impedance-meter. The sensing performance was evaluated by using spiked water contaminated by benzoquinone at a concentration level typical for industrial processes.

The structure of the paper is the following. In Section 2, the fabrication and characterization of the graphitic films are described. The fabricated PCB and the experimental EIS set-up and model are presented in Section 3. Section 4 deals with the testing results, aiming at demonstrating the feasibility of the proposed approach. The conclusions are summarized in Section 5.

2. Materials and Methods

2.1 Nanomembranes fabrication

Graphitic nanomembranes were fabricated on 1 inch 0.5 mm thick fused silica (SiO_2) wafers, by using ready-to-scale chemical vapour deposition (CVD) or pyrolysis methods.

Multilayer Graphene (MLG) was fabricated via CVD with CH_4: H_2 mixture in static atmosphere on the top of SiO_2 substrate plated with 10 nm-thick thermally evaporated nickel as the catalytic layer. Samples were pre-annealed for 2 hours in 20 sccm of hydrogen. Temperature was raised to 1000 °C in 60 minutes, when 40 sccm of CH_4 was added for 1 minute and was dwelled for 30 minutes. After the process, H_2 was added (10 mBar) for an overnight cooling.

Pyrolytic Carbon (PyC) film was synthesized by a CVD process at 1100 °C by using methane (CH_4:H_2) mixture as a carbon precursor, as described in [25]. The synthesis was carried out in static atmosphere. A CVD chamber was heated to 700 °C, at the rate of 20°C/min in 10mbar H_2. A quantity of 50 sccm of CH_4 was introduced in the chamber for 1 minute (50 sccm) and the temperature was further increased to 1100 °C at 10°C/min, to start methane decomposition. At this temperature, it was dwelled for 5 minutes and then cooled down to 700 °C at 5 °C/min. The CH_4 – H_2 atmosphere was replaced by H_2 at 700 °C (10mBar) for an overnight cooling.

Pyrolyzed Photoresist Films (PPF) with and without Ni catalytic layer were fabricated following the routes developed in [24]. Briefly, first 300µl of nLoF resist (AZR 1:4) were deposited on SiO_2 wafer through spin coating at 3000 rpm for 60 seconds, followed by 1 minute bake at 110 °C. The samples were then heated from 100 °C to 700 °C in an inert atmosphere at a rate of 20°C/min, and from 700 °C to 800 °C at 10°C/min. After, they were annealed for 30 minutes and cooled down in a static hydrogen overnight. The same procedure has been followed for the fabrication of graphitized PPF (PPF+Ni). However the nLof resists was deposited on a SiO_2 substrate, pre-covered with 10 nm thick catalytic Ni layer [24].

2.2 Nanomembranes characterization

The structural properties of fabricated graphitic films were characterized by Raman spectroscopy (Renishaw InVia Spectroscope with 514 nm excitation wavelength), optical transmittance (a spectrophotometer Perkin Elmer Lambda 1050 with integrating sphere), and scanning electron microscopy (SEM-LEO 1550 Gemini) (see the results in the Supplementary materials). The Raman spectra of the fabricated membranes correspond to graphitic materials of different level of crystallinity. Specifically, we fabricated:

(i) two amorphous films, PyC and PPF having similar Raman spectra. A slightly higher ratio of D to G peaks intensities in PyC vs that observed for PPF indicates a presence of more defects in the PyC structure.

(ii) two types of highly crystalline samples, MLG and PPF+Ni, show a presence of 2D peak and 2D/G intensities ratio corresponding to multilayer graphene. It is supported by the analysis of the optical transmittance spectra (Figure S3, Supplementary materials) indicating that MLG comprises of more than two graphene layers.

Full width half maximum, Raman shift and normalized intensities of graphitic films grown on fused silica are presented in Table S1 (Supplementary materials).

The sheet resistance, measured by home-made four-point probe set-up, varies from 0.076 (for PPF+Ni) to 195.1 kΩ/sq (for the MLG), which is sufficient for using them in EIS.

2.3. Atomic force microscopy

The correlation between morphology and Volt-Potential characteristics of nanomembranes was studied using Atomic Force microscope (Multimode 8, Bruker, USA) in the Kelvin Probe Force Microscopy (KPFM) mode, which employs a two-step technique. During the first step, measurements are performed in the semi-contact regime, which enables the mapping of the film topography (surface roughness). The probe-sample interaction are registered during the second step, which is performed in the non-contact regime by keeping the same (lift) distance between the probe and the sample surface. The lift distance is determined by the roughness.

All samples were studied by the PFQNE-AL conductive probe, whose resonant frequency is ~300 kHz, spring constant is ~0.8 N/m, and tip radius is ~5 nm. The cantilever and tip were fabricated from silicon nitride and silicon, respectively. The scan size was 10 µm and 4 µm. The scan resolution was 256×256 pixels, tip scan rate was 0.250 Hz.

The AFM image of the PyC film surface (Figs.1a,b) corresponds to an amorphous material of low porosity with embedded small (diameter < 40 nm) spots of crystalline carbon. The surface is smooth, and the topography contrast varies in the range of 15 nm. The PPF (Fig.1c,d) is also a low porous material with small spots (diameter is ~100 nm). The surface of samples with Ni is more developed and rougher than that non-comprising Ni catalytic buffer layer at the synthesis/fabrication stage (Figs.1a-d vs Figs.1e-h). Ni addition decreases the number and increases the size of the spots on the surface. The film roughness is given in Table 1.

Table 1. Average roughness (Ra) and root mean square roughness (RRMS) of the samples.

Sample	R_a, nm	R_{RMS}, nm
PyC	1.65	2.08
MLG+Ni	29.37	36.97
PPF	0.48	0.62
PPF+Ni	21.18	28.03

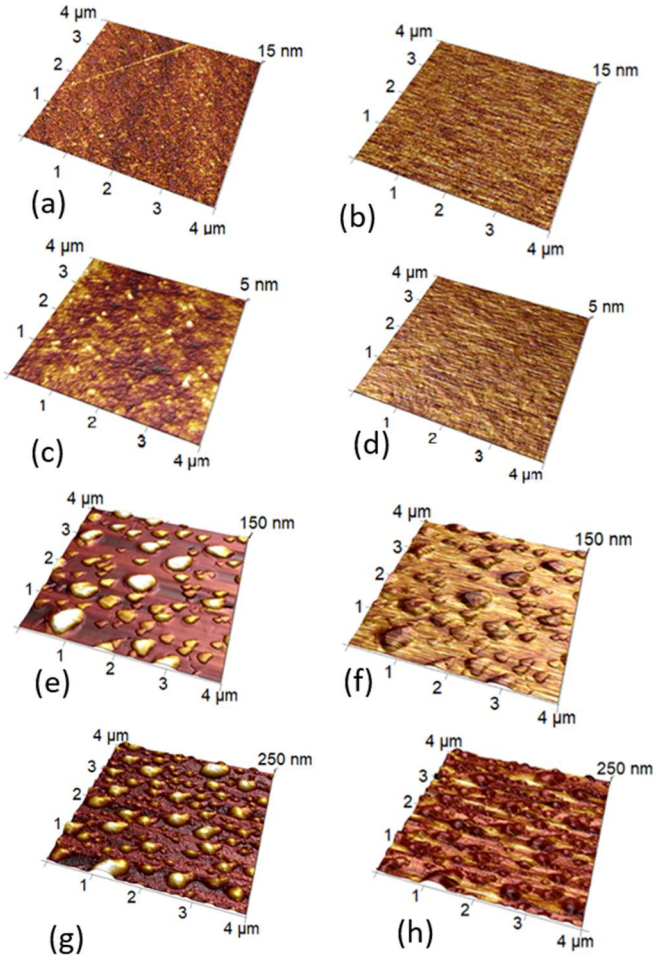

Figure 1: AFM images (a) topography of PyC in 3D (b) potential skin put on topography 3D with potential contrast from – 3.8 V up to – 1.5 V (c) topography of PPF in 3D (d) potential skin put on topography 3D with potential contrast from – 3.3 V up to – 1.1 V (e) topography of PPF+Ni in 3D (f) potential skin put on topography 3D with potential contrast from – 3.2 V up to – 0.35 V (g) topography in 3D of MLG (h) potential skin put on topography 3D with potential contrast from – 3.1 V up to – 0.15 V. Scan size is 4 µm. The. The scale ratio of Z axis versus X and Y axes is in real coordinates.

Given the tip radius (~5 nm), the surfaces of PyC and PPF films are found to be very smooth.

AFM data revealed the different adhesion of the membranes to the SiO_2 substrate (Fig. 2). From the most to the least adhesive ones according to the adhesion strength, the samples are distributed as follows: PyC (force spread is approx. 500 mV), MLG (1.1V), PPF (2.5V), PPF + Ni (11 V).

All samples were compared in terms of the potential by using depth histograms. Figure 3 shows the measured potential in volts referred to the probe potential level. One can observe that all the samples have almost the smallest potential difference except multi-layered graphene, which demonstrates a 3 times higher potential difference. This indicates a significant inhomogeneity of the samples' surface, that might influence the sensing response of MLG membranes.

To summarize, in terms of surface properties, i.e. uniformity and adhesion, PyC and PPF are the better choices for further use in industrial sensing applications.

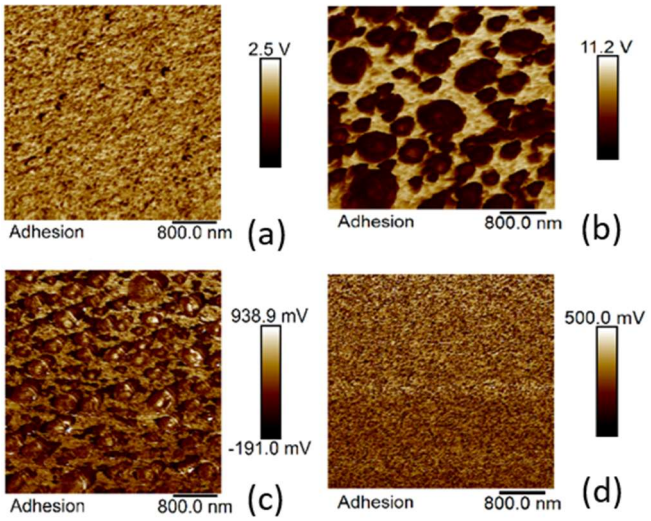

Figure 2: AFM image of Adhesion of (a) PPF (b) PPF+Ni (c) MLG. Scan size is 4 µm.

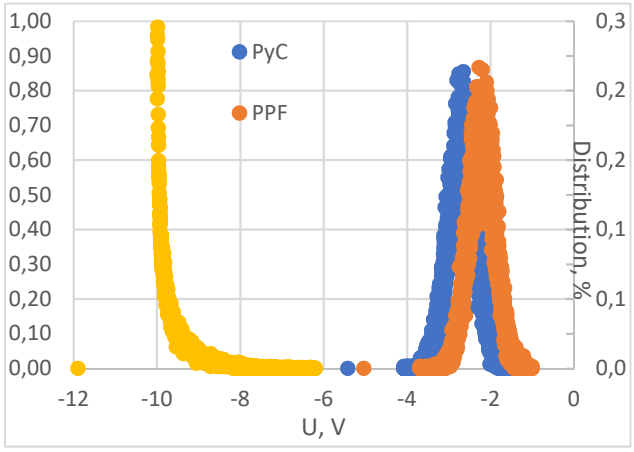

Figure 3: Depth histograms of samples´ potential.

3. Electrical Impedance Spectroscopy

The EIS technique proposed here is based on the time-domain measurements of the electrical impedance spectrum. In practice, the temporal evolution of the impedance at several frequencies is measured. The adopted set-up (Fig.4a) was made by an ad-hoc test-fixture hosting the membranes, connected to a bench impedance analyzer (GW Instek lcr 8110g Precision LRC meter). The test-fixture included two electrodes in contact to the membranes. The electrodes were put in the inner layer of a printed circuit board (see Fig.4a, right), to avoid the direct contact between them and the polluted water, that may affect the measured impedance. The electrodes were connected to the impedance analyzer by two cables, realizing the typical set-up of a 2-probe impedance measurement. Indeed, the expected level of the impedance (≈kΩ) made no necessary the use of the 4-probe technique.

The equivalent circuit model describing the above set-up is given in Fig.4b: the membrane was described as a series impedance $Z_S = R_S + iX_S$, whereas all the contributions coming from the setup (test-fixture, transitions, cables) were included in the parasitic components R_P, L_P, and C_P. The latter were compensated and removed at the beginning of each test campaign, by means of a preliminary calibration (open/short). Specifically, in the short procedure, a copper disk was inserted between the electrodes inside the test-fixture. The impedance measured for all frequencies in this condition was used to estimate the overall parasitic resistance R_P and parasitic inductance, L_P.

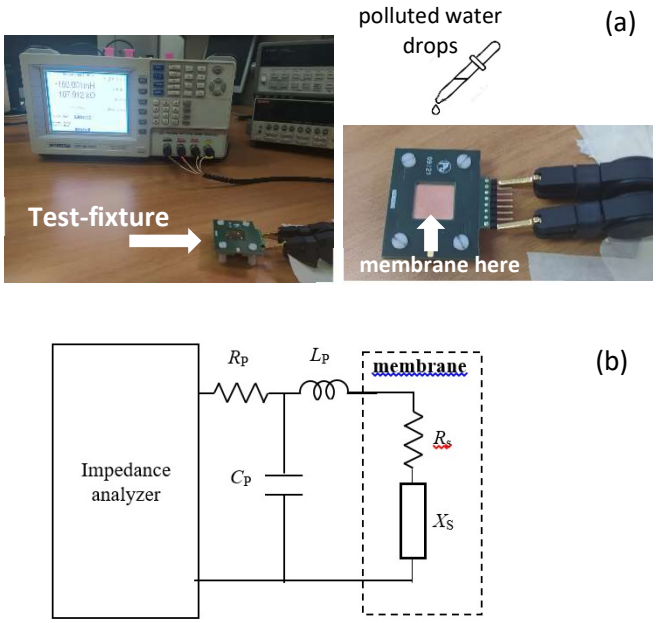

Figure 4: The EIS set-up: (a) pictures of the set-up with the membrane inserted into a test-fixture, connected to the impedance-meter; (b) equivalent circuit model of the set-up.

Next, an open circuit calibration was performed, by leaving the electrodes open, with insulating dielectric between them (FR4 dielectric). This calibration phase allowed evaluating and compensating the overall parasitic capacitance, C_P.

After this preliminary phase, these parasitic components were then removed by the impedance meter during the measurement process.

The experiments were conducted with benzoquinone, an oxidant widely used in organic synthesis. To check realistic conditions, the tests were performed by using 5 mM solution of pure benzoquinone in water. This concentration is typically found in polluted waste waters coming from industrial processes where this substance is used.

After inserting a membrane into the test-fixture, the time evolution of the impedance was measured for a suitable time interval in absence of any pollutant (so providing the baseline measurement). Then, a controlled quantity of polluted water (0.5 ml) was dropped on the membrane, and the time evolution of the impedance was recorded for a long-time interval, stopping at 3500 s. Then, the membrane was replaced, and the experiment was repeated. For each material, two different samples have been tested in different moments, to verify the reproducibility of the results.

4. Results and discussion

The temporal evolution of the electrical impedance at different frequencies was measured for each membrane with the set-up and the procedures described in Section 3.

4.1 The sensing system made by PyC membranes

The temporal evolution of the real (R) and imaginary (X) parts of the impedance for two PyC membranes is shown in Fig. 5, with reference to both samples. One can observe that as soon as the drops of polluted water hit the surface, both the resistance and the reactance significantly change, thus demonstrating the ability of the sensing system of realizing a real-time detection.

By comparing Figs.5a,b (sample 1) and Figs.5c,d (sample2) we can observe the same qualitative behavior: (i) the higher is the frequency, the bigger is the relative change of R and X, (ii) the relative change of R is lower than that of X; (iii) the baseline values (before the adsorption) are slightly different and show a weak frequency dependence; (iv) the steady-state values of R and X (after complete adsorption) show a pronounced frequency dependence.

The revealed dependence of R and X on adsorbent would be sufficient to propose a detection strategy based on monitoring their variations in time domain. However, observations (iii) and (iv) suggest a detection approach based on the evaluation of the frequency spread observed in the values of R and X, after and before the pollutant adsorption.

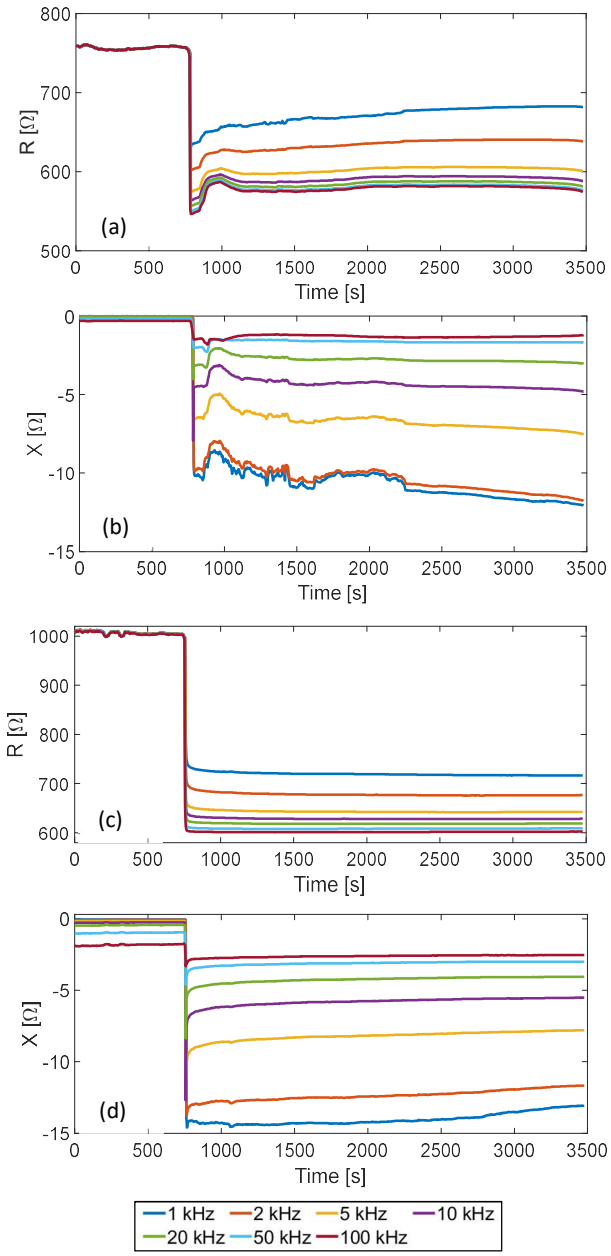

Figure 5: Time evolution of the real (R) and imaginary part (X) of the impedance of the PyC membrane, for 7 different frequency values: (a)-(b) sample #1; (c)-(d) sample #2. The polluted water was dropped at *t* = 750 s.

Note that the latter strategy can easily compensate the variations of the baseline due to sample fabrication and/or to ageing effects, as discussed later.

An alternative analysis may be carried out by plotting the results in the X-R plane (i.e., by observing the Nyquist plot X vs R). Figure 6 shows the Nyquist plot for sample #1 at three-time instants: before adsorption (Fig.6a); during adsorption (Fig.6b) and after complete adsorption (Fig.6c). In absence of pollutant (Fig. 6a), the Nyquist plot reduces down to

approximately a single point, showing that R and X are virtually frequency independent. As soon as the pollutant is injected (Fig. 6b), the Nyquist plot is transformed into a segment, because R and X begin to show frequency dependence. After the assessment time (Fig. 6c), the segment converted into a line, due to a pronounced frequency-dependence of R and X.

The frequency-spreads observed in Figs.5 and 6 allow us to introduce two figures of merit, in the following denoted as *maxdiff_R* and *maxdiff_X*. They quantify the time evolution of the frequency spread of the values of R and X, respectively, and can be used to estimate the sensing capability. They are defined as the difference between the maximum and the minimum values attained by R and X, at each time instant, t_n:

$$maxdiff\_R(t_n) = |\max_f[R(t_n)] - \min_f[R(t_n)]|, \quad (1)$$

$$maxdiff\_X(t_n) = |max_f[X(t_n)] - min_f[X(t_n)]|, \quad (2)$$

where the maximum and minimum refer to the frequency range: $1kHz \leq f \leq 100\ kH$.

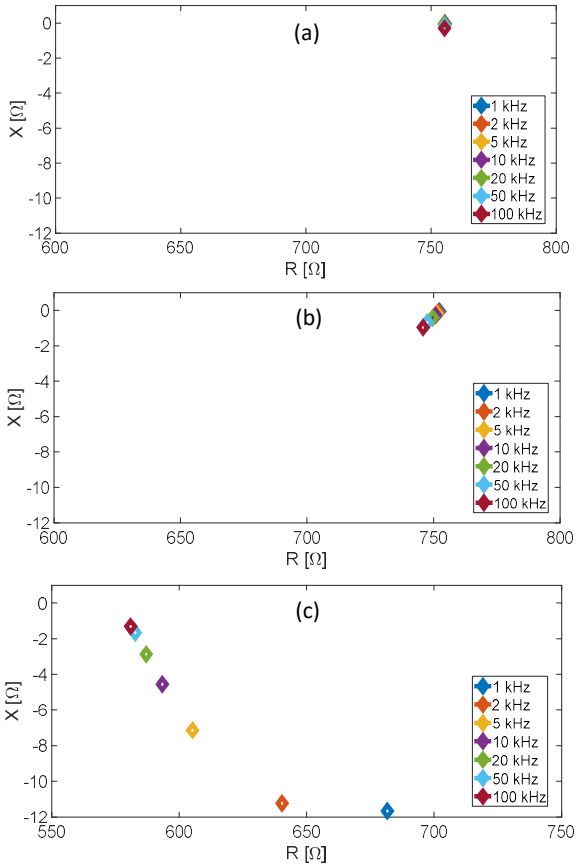

Figure 6. Measured values of reactance versus resistance (Nyquist plots) for the PyC membrane, sample 1, The values were taken at: (a) t = 410s (before adsorption); (b) t = 800s (adsorption right started); (c) t = 3000s (complete adsorption).

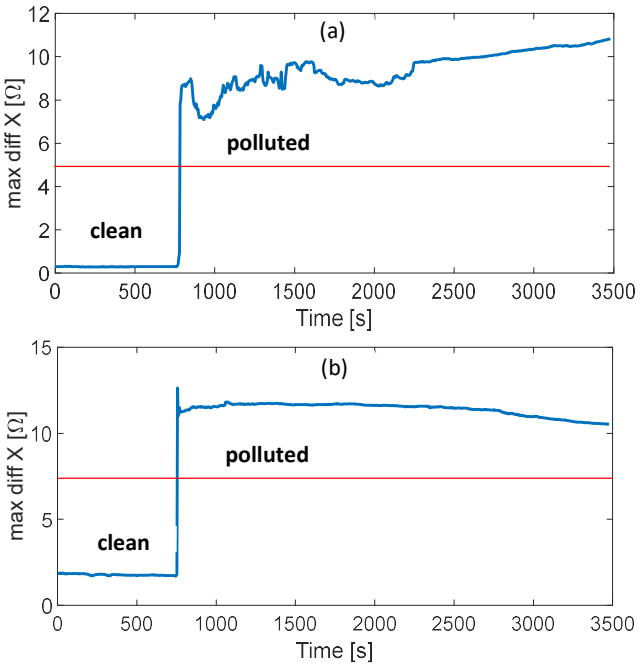

Figure 7: Time evolution of the figure of merit (2), evaluated for the PyC membrane: (a) sample 1; (b) sample 2. The pollutant is detected when this quantity overcomes the threshold (red line).

The time evolution of *maxdiff_X* is plotted in Fig. 7 for the two samples. Even though from one to another sample the baseline may change, the sharp and almost instantaneous variation of *maxdiff_X* as the polluted water is dropped suggests the possibility of easily identifying its presence. Indeed, a sensing threshold may be defined during the calibration phase (taking into account the baseline) and the detection occurs when *maxdiff_X* overcomes such a threshold.

These results demonstrate that the proposed sensing system enables a detection strategy that is independent on the absolute magnitude of the signals, being related only to the signal differences. Indeed, the signal magnitude may change, even in absence of the pollutants (baseline, i.e. initial impedance) for several reasons, including fabrication uncertainties (variations of the membrane properties due to reproducibility issues) or ageing effects. Therefore, the proposed approach provides a robust strategy that can compensate these issues.

In order to quantitatively estimate the detection resolution, the following "sensing parameters" have been defined and calculated from the proposed figures of merit:

i) σ_u: standard deviation in the time interval when the membrane is clean. This parameter represents the intrinsic noise of the sensor and is related to the measurement resolution. Specifically, in presence of the pollutant, differences from the baseline lower than three times σ_u should not be associated to the pollutant, but rather to the

sensor noise, while larger variations could be due to the presence of the pollutants.

ii) σ_P, standard deviation in the time interval when the membrane has completely adsorbed the pollutant. This parameter, if compared to σ_u, can give information about the presence of the pollutant on the membrane. If the pollutant would be removed, this value should tend to σ_u.

iii) D_T, "death time". This is the time needed to reach the 10% of the regime response (after the pollutant injection), starting from a value given by the mean value of the baseline plus $3\sigma_u$. During this time, the response does not provide reliable measurements on the pollutant.

iv) R_T, "rise time". This is the time needed to pass from the 10% to the 90% of the regime response. This time estimates the response of the sensor in presence of pollutant and gives information on the sensor bandwidth.

The parameters σ_u and σ_P are indexes of the sensing resolution, in absence or in presence of pollutants. Consequently, they are also associated to an estimation of the achievable limit of detection. The lower their values, the better the sensing performance. The parameter D_T is related to the sensitivity of the membrane. The lower its value, the higher the capability of the membrane of a fast detection of the pollutant. The parameter R_T is related to the bandwidth of the membrane when acting as a sensor. The lower its value, the higher the capability to follow rapid changes in the pollutant concentration.

Table 2 shows the values of the above parameters for the PyC (sample #1). By comparing these values with the results reported in Fig.7a, it is evident that the variation experienced by *maxdiff_X* right after the polluted water absorption is much higher than $3\sigma_u$. In addition, it can be noted that the value of σ_p is about one order of magnitude larger than σ_u.

Finally, to validate the proposed approach, the detection of the pollutant was also performed by using an alternative technique, namely the Cyclic Voltammetry (CV), by using graphene-modified screen-printed electrodes. When using this technique, drops of aqueous benzoquinone solution were placed on electrodes and the current between electrodes was recorded as a function of the applied potential (in the range from -1.5V to 1.5V, with a scan rate of 50 mV/s). The results of the CV are shown in Fig.8a for pollutant concentration from 2.5 to 80 mM.

One can observe from Fig. 8b that, at the benzoquinone concentration of 5 mM, the current peaks are hardly detectable, i.e. this concentration is close to the detectability limit of the CV technique.

Thus, we can conclude that the proposed EIS system is able to detect the presence of a very low concentration of the organic pollutant, demonstrating a performance comparable to the best systems based on electrochemical methods.

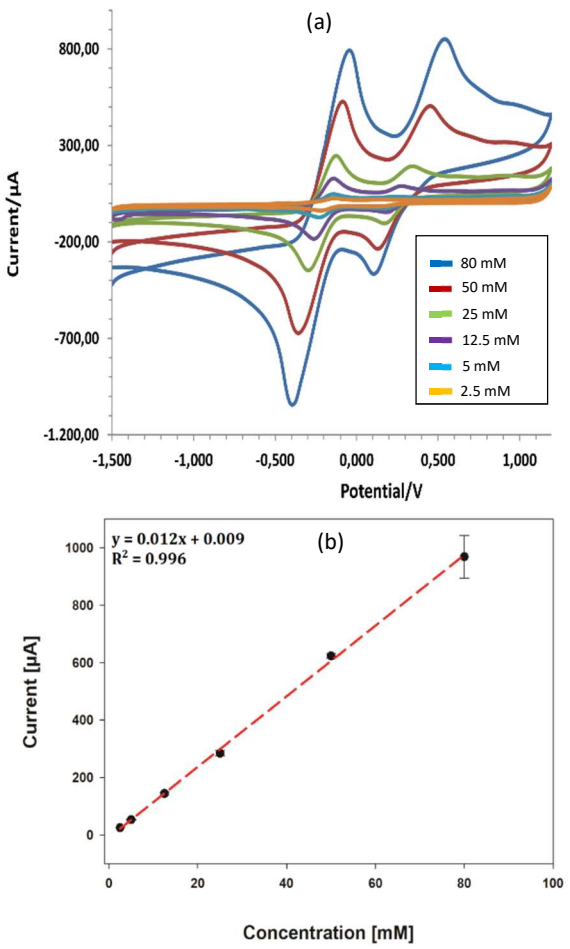

Figure 8: Cyclic Voltammetry detection of benzoquinone in water at different concentrations: (a) I-V responses; (b) maximum current peak vs concentration.

4.2 Performance of the other graphitic membranes

The same approach was applied to the other membranes described and characterized in Section 2, namely PPF+Ni, PPF and MLG+Ni films. The complete results related to these membranes are reported in the supplementary material. Here we only report the time behaviour of the figure of merit (2) for each of them, see Fig.9. The response of the PPF+Ni film (Fig.9a) exhibits the same qualitative behaviour as the PyC one, so also these membranes can effectively be used as sensing elements in the proposed EIS system.

Table 2 shows the values of all the sensing parameters obtained for the PPF+Ni membrane. Looking at these results and comparing them to those related to the PyC membrane, it can be highlighted as the PPF+Ni globally shows better performance. Indeed, such a film outperforms the PyC one for almost all parameters, warranting better sensitivity, promptness in the detection and bandwidth. Only the bandwidth referred to Max_diff_R shows worse performance .

Table 2. Estimated values of the sensing parameters for the PyC and PPF+Ni membranes.

Membrane	Parameter	Max_diff_R	Max_diff_X
PyC	σ_u [Ω]	0.77	0.022
	σ_p [Ω]	4.5	0.34
	D_T [s]	9	15
	R_T [s]	1.7	509
PPF+Ni	σ_u [Ω]	0.0069	0.0011
	σ_p [Ω]	0.12	0.0055
	D_T [s]	1.29	0.62
	R_T [s]	10.9	5.85

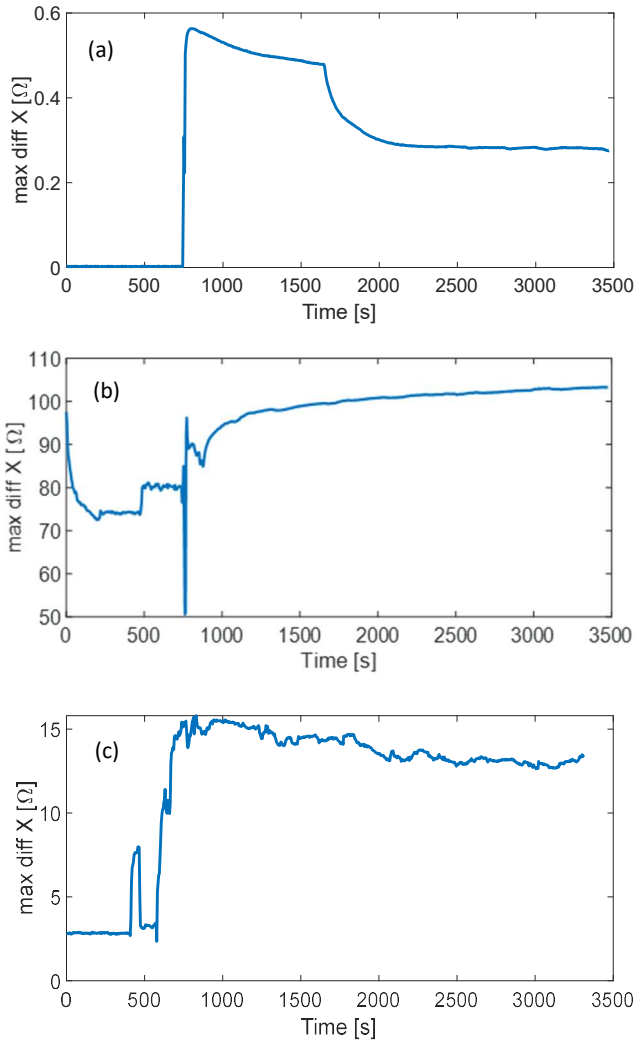

Figure 9: Time evolution of the figure of merit (2), evaluated for: (a) PPF+Ni; (b) PPF, and (c) MLG+Ni membranes.

Instead, the results obtained with the PPF and the MLG+Ni membranes (Figs.9b and 9c), suggest that these materials are less suitable for our purposes. Indeed, for PPF the figure of merit does not significantly change before and after the pollutant injection (Fig.9b). As for MLG+Ni film, the related figure or merit shows a non-monotonic behaviour (a peak) after the pollutant injection, that makes impossible to apply the proposed detection method (Fig.c) .

5. Conclusions

We demonstrated the feasibility of the water pollution monitoring via detecting the variation of the electrical impedance of graphitic nanomembranes. We examined membranes made of photoresist pyrolyzed (fabricated with and without presence of Ni catalyst layer), pyrolytic carbon and multi-layered graphene, which were deposited on integrable silica substrates by using simple, reproducible and scalable synthesis/fabrication processes. Structural and morphological parameters of those membranes that determine the sensor performance have been analysed.

The performance tests were carried out by using water contaminated by benzoquinone. This organic pollutant is challenging for alternative in-situ monitoring techniques like those based on voltammetry. The proposed technique was shown to be able to easily detect the presence of a small concentration of pollutant in water (5 mM). That is, the proposed approach offers a sensitivity comparable with that achieved in sensors based on the cyclic voltammetry technique.

Starting from the time evolution of the real and imaginary parts of the membrane impedance, we introduced figures of merit and sensing parameters that allow us to quantify and compare the performance.

The most promising membranes in terms of sensing properties are pyrolytic carbon and photoresist pyrolyzed with nickel catalyst layer.

By comparing the potential difference within all graphitic samples measured by AFM vs their sensing performance, one may conclude that, for the focus application, the lower the potential difference, the better the sensing performance. The only sample with high potential difference, i.e. MLG, does not demonstrate satisfactory sensing response. Moreover, we come to the interesting conclusion that highly developed surface and substantial roughness are not needed for an effective EIS-based sensing system.

Taking into account the best adhesive properties, as well as the exceptional uniformity of PyC along with its EIS response, we conclude that pyrolytic carbon the material to be integrated into ad-hoc printed circuit board. This will enable a prototype of a sensor capable to continuously monitoring the pollutants in water.

The obtained results can be considered as a first encouraging step towards the development of an advanced platform for the real-time and in-situ monitoring of contaminants in water. Future work will be devoted to a complete characterization of the sensor, aiming at (i) checking its dynamic response to the pollutant concentration; (ii) assessing reproducibility and repeatability of the results; (iii)

studying ageing effects; (iv) studying the selectivity of the response to different classes of pollutants. To this end, it is worth to be noted that the selectivity of the proposed 2D materials could be strongly improved by suitable functionalization processes.

Acknowledgements

This work is supported by NATO SPS Project "2DSENSE" and by the Academy of Finland via Flagship Programme Photonics Research and Innovation (PREIN), decision 320166, and grant 343393. P.K. is supported by Horizon 2020 IF TURANDOT project 836816. The Authors acknowledge Dr. Alessio Di Tinno and Prof. Erkki Lähderanta for their contribution in preparing the pollutant solutions and preparation of the manuscript.

References

[1] Nakamura H 2010 Recent organic pollution and its biosensing methods Anal. *Methods* **2** 430-444

[2] Meyer A M, Klein C, Fünfrocken E, Kautenburger R, Becka H P 2019 Real-time monitoring of water quality to identify pollution pathways in small and middle scale rivers *Science of the Total Environment* 651 2323-2333.

[3] Patel B R, Noroozifar M, Kerman K 2020 Nanocomposite-based sensors for voltammetric detection of hazardous phenolic pollutants in water *Journal of the Electrochemical Society* **167** 037568

[4] Power A C, Gorey B, Chandra S, and Chapman J 2018 Carbon nanomaterials and their application to electrochemical sensors: a review *Nanotechnology Reviews* **7** 19-41.

[5] Li Q., et al. 2021 Recent advances in black phosphorus-based electrochemical sensors: A review *Analytica Chimica Acta*, **1170** 338480.

[6] Liu H, Xiong R, Zhong P, Li G, Liu J, Wu J, Ying L, Quanguo H 2020 Nanohybrids of shuttle-like α-Fe2O3 nanoparticles and nitrogen-doped graphene for simultaneous voltammetric detection of dopamine and uric acid *New Journal of Chemistry* **44** (47) 20797-20805

[7] Li G, Xia Y, Tian Y, Wu Y, 2019 Review: Recent Developments on Graphene-Based Electrochemical Sensors toward Nitrite *Journal of The Electrochemical Society* **166**(12) B881-B895

[8] Peng H, Yu Q, Wang S, Kim L, Rowan A E, Nanjundan A K, Yamauchi Y, Yu J 2019 Molecular Design Strategies for Electrochemical Behavior of Aromatic Carbonyl Compounds in Organic and Aqueous Electrolytes *Advanced Science* **6**(*17*) 1900431.

[9] Bielicka-Daszkiewicz K, Krawczyk P, Nowicka K 2012 Examination of benzoquinone electrooxidation pathway as crucial step of phenol degradation process *Electrochimica Acta* **80** 22-26.

[10] Han C, Ye Y, Wang G, Hong W, Feng C 2018 Selective electro-oxidation of phenol to benzoquinone/hydroquinone on polyaniline enhances capacitance and cycling stability of polyanilineelectrodes *Chemical Engineering Compounds* **347** 648-659.

[11] Muñoz J, Montes R, Baeza M 2017 Trends in electrochemical impedance spectroscopy involving nanocomposite transducers: Characterization, architecture surface and bio-sensing *Trends in Analytical Chemistry* **97** 201-215.

[12] Ferrigno L, Cataldo A, Sibilia S, Maffucci A, Bellucci S 2020 A Monitorable and Renewable Pollution Filter Based on Graphene Nanoplatelets *Nanotechnology* **31** 075701.

[13] Miele G, et al. 2021 Electrical Impedance Spectroscopy for Real-Time Monitoring of the Life Cycle of Graphene Nanoplatelets Filters for Some Organic Industrial Pollutants, *IEEE Trans. on Instrumentation and Measurement (early access)*, DOI: 10.1109/TIM.2021.3089247.

[14]Bellucci S, Cataldo A, Ferrigno L, Giovannetti S, and Maffucci A 2020, An Impedance-Based Life-Monitoring Technique for a Graphene Water Filter *Lecture Notes in Electrical Engineering, Springer* **604** 719-726.

[15]Anichini C, et.al. 2018 Chemical sensing with 2D materials *Chem. Soc. Rev.* **47** 4860.

[16] Beitollahi H, Mohammadi S Z, Safaei M, and Tajik S 2020 Applications of electrochemical sensors and biosensors based on modified screen-printed electrodes: a review *Anal. Methods* **12** 1547–1560.

[17]Todri-Sanial A, Dijon J, Maffucci A 2016 *Carbon nanotubes for interconnects: Process, design and applications* Springer, The Netherlands, ISBN: 9783319297446.

[18]Sibilia S, Bertocchi F, Chiodini S, Cristiano F, Ferrigno L, Giovinco G, Maffucci A 2021 Temperature-dependent electrical resistivity of macroscopic graphene nanoplatelet strips *Nanotechnology* **32**(27) 275701.

[19] Zhao G, Li J, Ren X, Chen C, and Wang X 2011 Few-layered graphene oxide nanosheets as superior sorbents for heavy metal ion pollution management *Environ. Sci. Technol.* **45** 10454–10462.

[20] Yang S Y, Vecitis C D, Park H 2019 Electrocatalytic water treatment using carbon nanotube filters modified with metal oxides *Environmental Science and Pollution Research* **26** 1036–1043.

[21] Akbari A, et al. 2016 Large-area graphene-based nanofiltration membranes by shear alignment of discotic nematic liquid crystals of graphene oxide *Nature Communications* **7** 10891.

[22] Huang H, Song Z, Wei N 2013 Ultrafast viscous water flow through nanostrand-channelled graphene oxide membranes *Nat. Commun.* **4** 2979.

[23] Wu Y, Zhu J and Huang L 2019 A review of three-dimensional graphene-based materials: Synthesis and applications to energy conversion/storage and environment *Carbon* **143**, 610-640.

[24] Baah M, Obraztsov P, Paddubskaya A, Biciunas A, Suvanto S, Svirko Y, Kuzhir P, and Kaplas T 2020 Electrical, transport and optical properties of multifunctional graphitic films synthesized on dielectric surfaces by nickel nanolayer assisted pyrolysis, *ACS Appl. Mater. Interfaces* **2020**, 12, 5, 6226-6233.

[25] Batrakov K, Kuzhir P, Maksimenko S, Paddubskaya A, Voronovich S, Kaplas T, and Svirko Y 2013 Enhanced microwave shielding effectiveness of ultrathin pyrolytic carbon films, *Applied Physics Letters,* **103,** 073117.